TiO_2-Assisted Microstructural Variations in the Weld Metal of EH36 Shipbuilding Steel Subject to High Heat Input Submerged Arc Welding

YONGWU WU, XIAOBO YUAN, IMANTS KALDRE, MING ZHONG, ZHANJUN WANG, and CONG WANG

Two simple yet comparable fluxes, CaF_2 and CaF_2–40 wt pct TiO_2, have been employed to engineer shipbuilding steels under high heat input submerged arc welding, aiming to clarify the unique functions demonstrated by incurring TiO_2 addition. Compared with pure CaF_2, TiO_2-containing flux could increase columnar austenite width from 119.2 ± 18.1 to 201.5 ± 32.2 μm. Furthermore, TiO_2 could significantly enhance acicular ferrite fraction, which has been primarily enabled by the formation of Ti-bearing inclusions.

https://doi.org/10.1007/s11663-022-02697-x

HIGH heat input submerged arc welding (SAW), due to high deposition rate, has been widely developed for joining thick steel grades in the shipbuilding, offshore engineering, and pipeline industries.[1] However, high heat input could produce coarse yet brittle microstructural constituents in the weld metal (WM), thus deteriorating mechanical properties of the entire weldment.[2,3] To address such challenge, a proven strategy is to adjust welding flux composition to fine-tune WM microstructures for desired performances.[4–7]

One of the most effective ways is to introduce TiO_2 component into the flux, which will improve the O content of the WM, and invariably lead to the population of Ti-containing inclusions in sizeable quantities, thus significantly enhancing the presence of acicular ferrites (AFs) and end-user properties.[8–11] Kohno *et al.*,[12] by ushering TiO_2 into the CaF_2–Al_2O_3–SiO_2–BaO–CaO–MnO–MgO–B_2O_3 fluxes to weld high strength low alloy steel, clarified that the optimal low-temperature toughness at 213 K could be obtained when Ti content of the WM was 0.02 wt pct, which corresponded to 8 pct TiO_2 content. Similar results have also been reported by Zhang *et al.*[13] and Roy *et al.*[14] in EH36 low carbon low alloy steel treated by CaF_2–SiO_2–MgO–Al_2O_3–TiO_2 and CaF_2–SiO_2–MgO–Al_2O_3–MnO–TiO_2 fluxes, respectively. Moreover, the correlation of the thermo-physical properties of TiO_2-based fluxes with microstructure and mechanical properties of the WM was established by Kim *et al.*[15] It was revealed that both thermal conductivity and electronegativity of the fluxes can affect the arc heat transfer and eventually determine the microstructures of the WM. However, it needs to be pointed out that available studies are dwelled on multi-component and/or even commercial fluxes,[16,17] whose compositions are rather complicated, and possible impurities might obscure explanations of the roles played solely by TiO_2. In order to eliminate potential ambiguities, TiO_2-containing fluxes composed of minimal constituents are necessitated, particularly for high heat input applications.

In the present study, we design two simple yet comparable welding fluxes, with one being pure CaF_2, and the other being CaF_2–40 wt pct TiO_2, which are based on the following criteria by referring to the CaF_2–TiO_2 phase diagram and preceding investigations: (1) the melting temperature (1448 °C) shall be acceptable for welding operations; (2) oxygen content of the WM shall be in a suitable range.[4,18,19] By processing the EH36 shipbuilding steel using these two fluxes, microstructural features in the WMs are examined, and potential differences are elucidated with respect to the TiO_2 component. It is anticipated that current findings could shed light on the unique functions enabled by TiO_2, and potentially facilitate the design of welding fluxes geared for high heat input applications.

For the TiO_2-free flux, 1000 g of pure CaF_2 powders (> 98.5 mass pct, Sinopharm Chemical Reagent Co., Ltd., SCRC, China) were weighed. For the

YONGWU WU, XIAOBO YUAN, MING ZHONG, ZHANJUN WANG, and CONG WANG are with the Key Laboratory for Ecological Metallurgy of Multimetallic Mineral (Ministry of Education), Northeastern University, Shenyang 110819, Liaoning, P.R. China and also with the School of Metallurgy, Northeastern University, Shenyang 110819, P.R. China. Contact e-mail: wangc@smm.neu.edu.cn IMANTS KALDRE is with the Institute of Physics, University of Latvia, Riga 1004, Latvia.

Manuscript submitted July 12, 2022; accepted November 15, 2022. Article published online December 2, 2022.

TiO_2-containing flux, 600 g CaF_2 and 400 g TiO_2 (> 99.0 mass pct, SCRC, China) reagent-grade powders were mixed for 0.5 hours in the blender mixer. Afterwards, the well-mixed powders were melted at 1823 K for 1 hour in a graphite crucible with a graphite lid, and quenched with water at room temperature. The solidified particles of initial fluxes were dried, crushed, and sieved into 8 to 40 mesh, and finally baked at 973 K for 2 hours to remove moisture and potential graphite before welding. Chemical compositions of fluxes were determined by X-ray fluorescence spectroscopy (XRF, model S4 Explorer). Differences between nominal and analytical composition were within 5 pct and deemed as negligible.[9] Additionally, the valence state of TiO_2 is Ti^{4+} throughout the experiment as the entire welding experiment was performed in an open environment, which is also confirmed by FactSage calculations in previous investigations.[16,17,20]

Bead-on-plate SAW trials were carried out in the horizontal position of EH36 shipbuilding plates. EH36 steel plates were machined in a dimension of 800 mm × 250 mm × 24 mm. The welding parameters of the double-wire SAW were set to a welding speed of 500 mm/min, DC-850 A/32 V for welding wire forward, and AC-625 A/36 V for welding wire backward, to achieve the heat input of 60 kJ/cm. Metallic elements were analyzed by an inductively coupled plasma optical emission spectrometer (ICP-OES, 8300 DV, Perkin Elmer Optima). C and O were analyzed using a LECO analyzer (CS230 for C and ONH836 for O). WMs corresponding to CaF_2 and CaF_2–40 wt pct TiO_2 fluxes are marked as WM-0 and WM-40, respectively. Chemical compositions of EH36, welding wire, and WMs are summarized in Table I.

After welding, the specimens, normal to the direction of welding speed, were sectioned at three different locations of 5 cm each apart along the length of weld beads undergoing steady welding conditions. Subsequently, sectioned specimens were mechanically ground, polished, and etched for 10 seconds by a 4 pct Nital. Macro-morphological observation was conducted using an optical stereomicroscope (SZ61, Olympus, Japan). Columnar austenite grains were presented in the cross section,[21] and measured using the linear intercept method (ASTM E112-1996), in which the size of columnar austenite grain refers to the width between grain boundary ferrites, GBFs.[22] Microstructures (inclusions) were analyzed by scanning electron microscope (SEM, Tescan, MIRA3, Czech Republic) coupled with an energy dispersive spectrometer (EDS, Max 40, Oxford Instruments, UK). Volume fractions of distinct microstructural features were measured by the area method of the Image-Pro Plus 6.0 using 20 SEM images at 2000×.

Table I. Chemical Compositions of EH36, Welding Wire, and WMs (Weight Percent)

Elements	C	Mn	Si	Ti	Al	O
EH36	0.052	1.540	0.142	0.010	0.021	0.003
Welding wire	0.127	1.650	0.049	0.010	0.022	0.003
WM-0	0.081	1.510	0.114	0.004	0.014	0.004
WM-40	0.069	1.096	0.081	0.037	0.013	0.021

Figures 1(a) and (b) show the cross-sectional macrographs in WM-0 and WM-40. The width, depth, and reinforcement of WM-0 are measured to be 23.0, 7.5, and 2.3 mm, respectively. For WM-40, the width remains the same. However, it can be seen that the morphology has undergone significant changes, with the depth of penetration increasing to 9.2 mm and the reinforcement boosting to 6.2 mm. Furthermore, the profile of the reinforcement transforms from a flat-top (WM-0) to a well-developed arc shape. It is clearly demonstrated that TiO_2 addition alters WM geometry, which could be enabled by metal transfer behaviors as reported consistently by Sengupta *et al.*[1,23] and Cho *et al.*[24,25]

Besides TiO_2-induced morphological variations, another interesting phenomenon to notice is the change of columnar austenite grains, which are developed epitaxially from the fusion boundary (black dotted curves in Figures 1(a) and (b)) to the centerline of the WM. For WM-0, the interesting area shown in Figure 1(a) is further enlarged in Figure 1(c), where the columnar austenite grains are growing in a rather parallel yet straight manner. The average width of those columnar austenite grains is measured to be 119.2 ± 18.1 μm. As a contrast, columnar austenite grains in WM-40 are presented in Figure 1(d), indicating significant lateral expansion has taken place during grain formation. Correspondingly, the average grain width increases to 201.5 ± 32.2 μm. Such finding is consistent with previous investigations by Evans[26] and Zhang and Farrar.[22] This variation of columnar austenite grain could be ascribed to the synergistic effect of elemental changes induced by C, Mn, and Si, which can be described by Eq. [1]:

$$\overline{L}\ (\mu\text{m}) = 64.5 - 445.8(\text{wt. pct C}) + 139(\text{wt. pct Si}) - 7.6(\text{wt. pct Mn}) + Q\ (\text{heat input, kJ/cm}), \quad [1]$$

where $\overline{L}$ is the average width of columnar austenite grains. For WM-0, $\overline{L}$ is calculated to be 92.8 μm, which is fairly close to the measured value. However, for WM-40, the value of $\overline{L}$ is 96.7 μm, which is far lower than the measured value (201.5 ± 32.2 μm). The discrepancy could be resulted from the coarsening of columnar austenite grains during cooling after solidification. Compared with WM-0, higher reinforcement and deeper penetration of WM-40 promote heat accumulation in the WM,[24,25] leading to the lateral expansion of columnar austenite grains along the temperature gradient of the WM, which further affects the merging and growing of subsequent columnar austenite grains. This phenomenon has also been reported in the investigation of columnar solidification structures in laser or electron beam additive manufacturing.[27,28]

Figure 2 shows typical microstructures inside the columnar austenite grains of WM-0 and WM-40. For

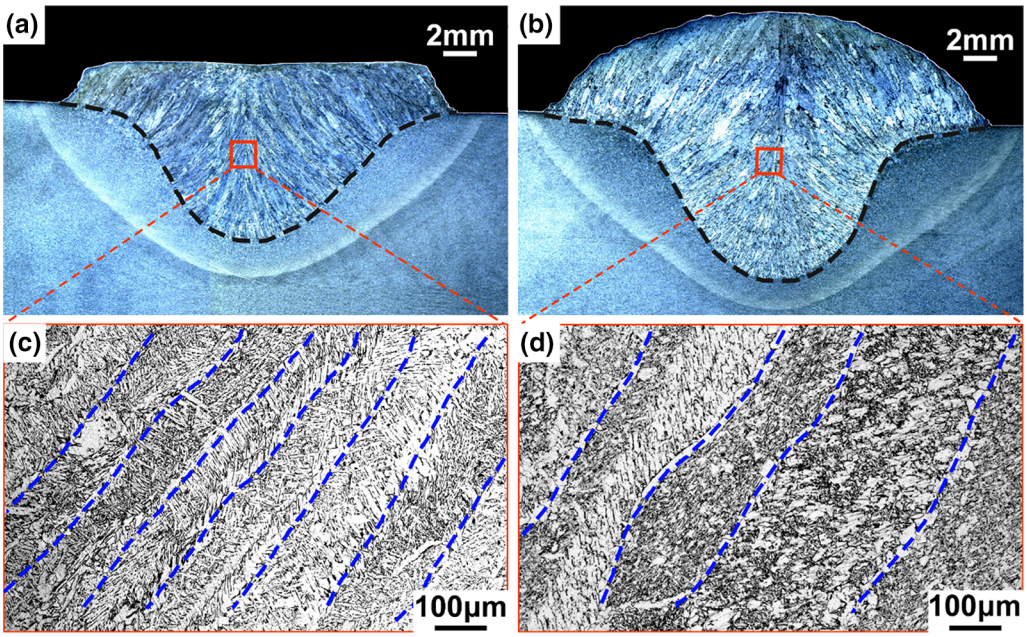

Fig. 1—Cross-sectional macrographs of: (*a*) WM-0 and (*b*) WM-40; enlarged columnar austenite grains of: (*c*) WM-0 and (*d*) WM-40 (red squares represent the observed zones magnified in (c) and (d), respectively, black curves represent the fusion boundary, and blue curves represent austenite grain boundaries) (Color figure online).

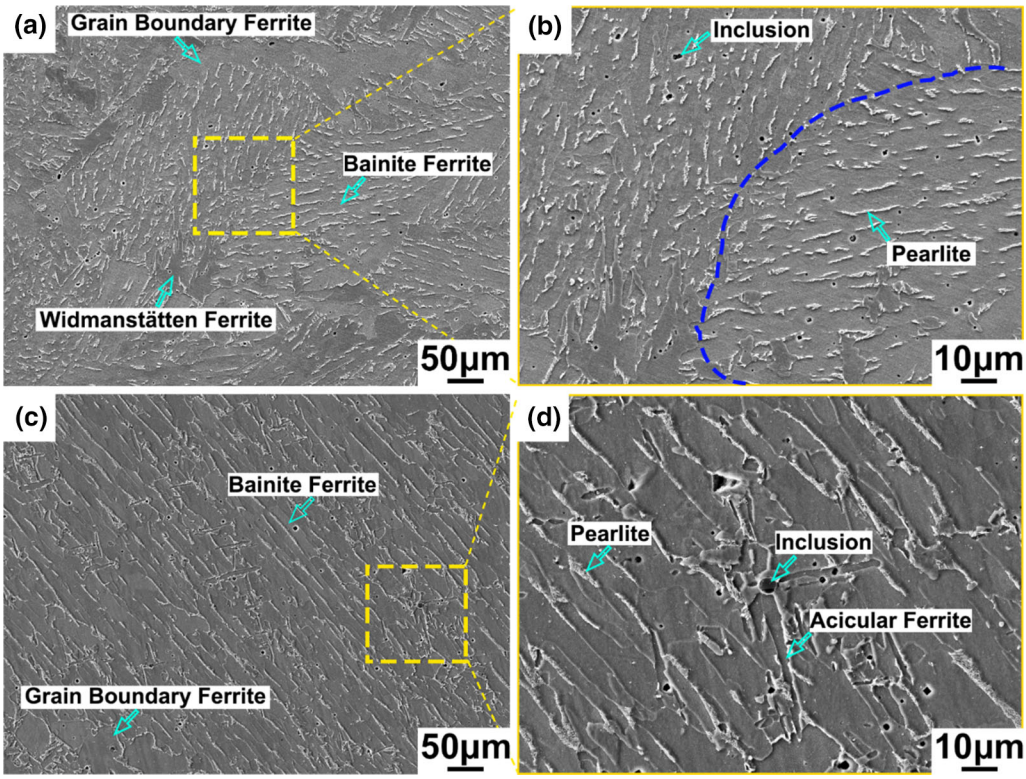

Fig. 2—Micrographs inside the columnar austenite grains of (*a*) WM-0, (*b*) enlarged area in (a), (*c*) WM-40, and (*d*) enlarged area in (c) (yellow rectangles represent enlarged area, and blue dotted curve indicates bainite block boundary) (Color figure online).

WM-0, as shown in Figure 2(a), microstructures are heterogeneous in nature and primarily comprised GBF, Widmanstätten ferrite (WF), and bainite ferrite (BF). It can be seen that wedge-shaped plates of WF grow from a certain thickness of GBF to the interior of grains. It is reported that WF might easily emanate from existing GBF by edge-to-face nucleation at a low cooling rate, which is inevitable for high heat input welding.[29,30] BF

plates with aligned pearlite (P) colonies nucleate from a continuous GBF occupied the entire grain boundary, and grow to the grain interior by sympathetic nucleation.[31,32] Moreover, from the enlarged interested area in Figure 2(a), it can be seen that BF plates impinge on each other to form BF packets within the grain, as marked by the blue curve in Figure 2(b). Additionally, dispersed inclusions appear to be engulfed by BF plates, but rarely induce the formation of ferrites. In WM-40, microstructures are dominated by BF and AF, as observed in Figure 2(c). BF plates possess the same growth behaviors as those of WM-0, but GBF is granular in shape and occupies prior austenite grain boundaries.[21,33] AF laths interlock with each other, and a certain number of them are directly associated with inclusions, as shown in Figure 2(d). In addition, AF laths intersect with BF plates, which might be enabled by post-grown BF plates passing through or bypassing already-grown AF laths.[34,35]

Figure 3 summarizes relative fractions of salient phases in WM-0 and WM-40. The most noteworthy variation is a sharp increase of the AF fraction from 3.0 ± 1.4 to 36.0 ± 2.6 pct, which is concurrent to the decrease of the BF fraction from 61.5 ± 0.7 to 44.7 ± 1.5 pct. The extensive population of AFs could be directly associated with inclusions, in which the cumulative increase of AF is further triggered on prior AF laths by sympathetic nucleation.[21,36] In turn, the increase of AF depresses BF within austenite grains. Meanwhile, the amount of GBF and WF, both nucleated mainly at austenite grain boundaries, decreases from 25.5 ± 0.7 to 13.3 ± 1.5 pct, and from 9.0 ± 1.4 to 6.0 ± 1.0 pct, respectively. The growth of WF is likely blocked by AFs in prior austenite grains, resulting in a slight decrease of its fraction from WM-0 to WM-40.[21,37]

Figure 4 shows typical inclusions and associated EDS spectra detected in WM-0 and WM-40. In WM-0, the typical inclusion has a size of 1.5 μm and is engulfed by BF plates (Figure 4(a)). It is seen from element analysis that chemistries of the inclusion are O (39.68 at. pct), Al (39.22 at. pct), Mn (12.48 at. pct), and Mg (8.62 at. pct), indicating the inclusion might have been formed in a complex manner.[38] As a sharp contrast, the counterpart in WM-40 is significantly larger in size, as shown in Figure 4(b), and corresponding chemistries are featured by Ti (74.61 at. pct), O (14.04 at. pct), Al (2.57 at. pct), and Mn (8.78 at. pct), suggesting inclusions could have been transformed to Ti-bearing category.[38] Another major feature is the presence of AF laths, which are triggered to form on the surface of a Ti-bearing inclusion, consistent with previous findings.[38,39]

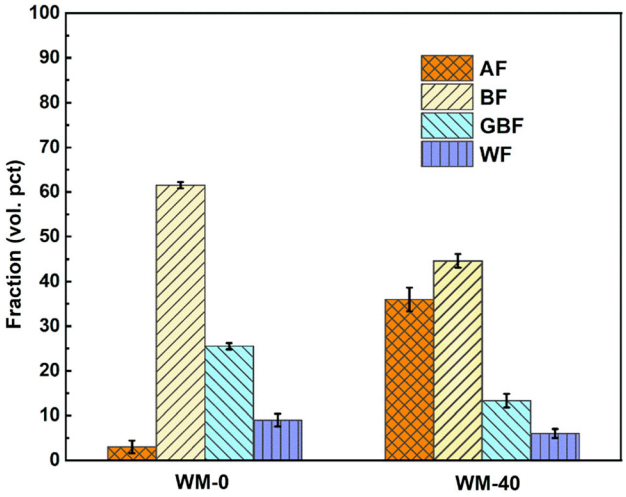

Fig. 3—Relative fractions of salient phases in WM-0 and WM-40.

It is clear that the addition of TiO_2 into the welding flux could impact the element transfer of Ti and O into the WM.[9,38] A plausible explanation suggests that such transfer behaviors should have been driven by arc interaction in SAW, which is given by Reaction [2].[20]

$$(TiO_2) \overset{arc}{=} [Ti] + 2[O]. \quad [2]$$

As a consequence, dissolved Ti and excessive soluble O could react to form TiO_x-bearing inclusions during solidification.[38,40] Moreover, it has been reported that Ti-bearing oxides tend to be formed as the weight ratio of Al to O is less than 1.0.[40,41] In the present work, the corresponding ratio of Al and O is 3.5 in WM-0 while that of WM-40 is 0.62, as presented in Table I, the latter of which provides a favorable condition for the formation of Ti-bearing inclusions, thus facilitating the formation of AF, as demonstrated in Figure 4(b).

Figure 5 shows a schematic illustration of microstructural variations induced by TiO_2 fluxes. The WM processed by TiO_2-free flux (CaF_2) is principally featured by GBF, WF, and BF, in which continuous GBF and coarse WF decorate preferentially prior austenite grain boundaries, and BF occupies the interior of columnar austenite grains.[21] After TiO_2 addition, as chemical compositions (especially C, Mn, Ti, O)[9,38] and WM geometry[24,25] have been drastically altered, columnar austenite grains in the WM are coarsened, which are accompanied by the formation of Ti-bearing inclusions, promoting the significant population of AF at the expense of other major microstructural constituents.

To summarize, microstructures of the WM of EH36 shipbuilding steel subject to 60 kJ/cm SAW have been investigated under two fluxes. Salient features have been characterized, and major conclusions are as follows:

(1) Compared with pure CaF_2, TiO_2-containing flux could increase columnar austenite width from 119.2 ± 18.1 to 201.5 ± 32.2 μm.
(2) Microstructural constituents in the TiO_2-free WM are composed of BF, WF, and continuous GBF, while those of TiO_2-treated WM are dominated by AF, BF, and granular GBF. The volume fraction of AF significantly increases, while that of BF diminishes.
(3) The addition of TiO_2 into welding flux could shift inclusion chemistry from Al–Mn–Mg–O dominating case to the Ti-bearing scenario, thanks to the transfer of Ti and O from the flux to the WM.

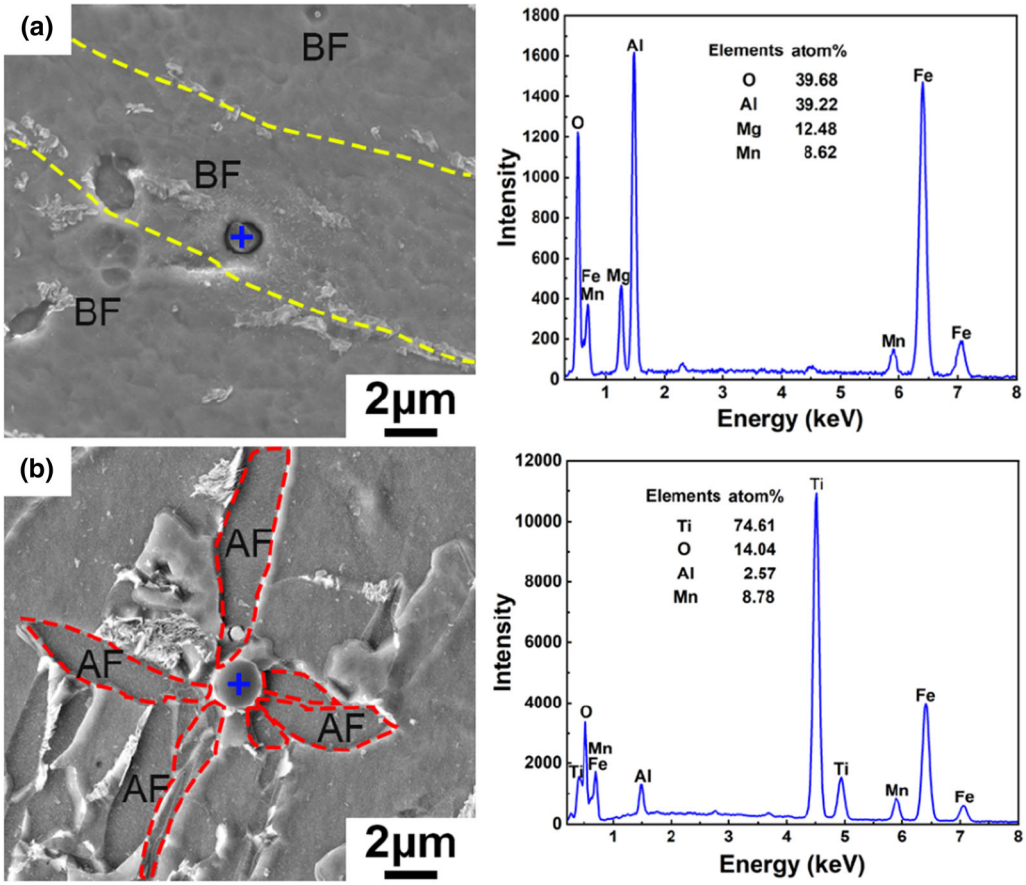

Fig. 4—Morphology, composition, and corresponding EDS spectra analysis of typical inclusions in (*a*) WM-0 and (*b*) WM-40 (blue cross indicates targeted inclusions for EDS, yellow curves mark grain boundaries of BF plates, and red dotted curves indicate AF) (Color figure online).

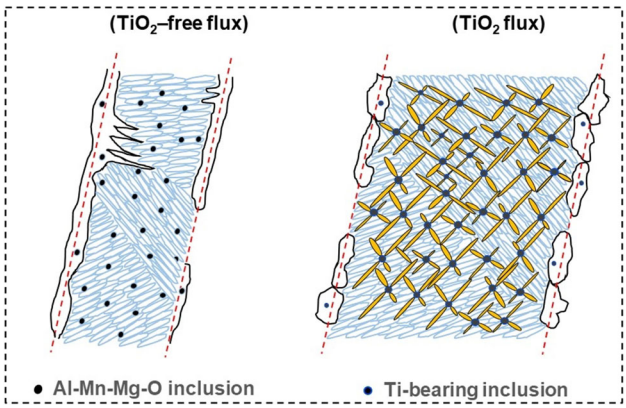

Fig. 5—Schematic illustration depicting microstructural variations of the WMs induced by TiO_2 flux (red lines represent the columnar austenite grain boundaries) (Color figure online).

ACKNOWLEDGMENTS

The authors sincerely acknowledge the financial support from National Natural Science Foundation of China (Grant Nos. U20A20277, 52011530180, 52050410341, and 52104295), and Research Fund for Central Universities (Grant Nos. N2125016 and N2025025).

DATA AVAILABILITY

All data generated or analysed during this study are included in this published article.

CONFLICT OF INTEREST

On behalf of all authors, the corresponding author states that there is no conflict of interest.

REFERENCES

1. B.V. Sengupta, D. Havrylov, and P.F. Mendez: *Weld. J.*, 2019, vol. 98, pp. 283s–313s.
2. K. Akihiko, Y. Kenichi, H. Tomohiko, S. Osamu, I. Kazutoshi, Y. Yuzuru, S. Yasumi, and A. Kiyosaburo: Nippon Steel Technology Report, 2004, pp. 33–37.
3. M. Minagawa, K. Ishida, Y. Funatsu, and S. Imai: Nippon Steel Technology Report, 2004, pp. 6–8.
4. C. Wang and J. Zhang: *Acta Metall. Sin.*, 2021, vol. 57, pp. 1126–40.
5. C.B. Dallam, S. Liu, and D.L. Olson: *Weld. J.*, 1985, vol. 64, pp. 140–51.

6. X.Y. Guo, L.F. Zhao, X. Liu, and F.G. Lu: *Int. J. Fatigue*, 2019, vol. 120, pp. 1–11.
7. N. Yan, S.F. Yu, and Y. Chen: *Sci. Technol. Weld. Join.*, 2015, vol. 20, pp. 418–24.
8. D.L. Olson, S. Liu, R.H. Frost, G.R. Edwards, and D.A. Fleming: *Nature and Behavior of Fluxes Used for Welding*, ASM International, Materials Park, OH, 1993, pp. 43–54.
9. J. Zhang, T. Coetsee, H.B. Dong, and C. Wang: *Metall. Mater. Trans. B*, 2020, vol. 51B, pp. 1953–57.
10. X. Xie, M. Zhong, T. Zhao, and C. Wang: *Sci. Technol. Weld. Join.*, 2022, vol. 27, pp. 472–78.
11. K.M. Kumar, P.V.G. Krishna, and K. Kishore: *Mater. Today Proc.*, 2020, vol. 22, pp. 2300–05.
12. R. Kohno, N. Mori, K. Nagano, and T. Takami: *Weld. J.*, 1982, vol. 12, pp. 373s–80s.
13. J. Zhang, T. Coetsee, S. Basu, and C. Wang: *CALPHAD*, 2020, vol. 71, p. 102195.
14. J. Roy, R.N. Rai, and S.C. Saha: *Int. J. Mater. Prod. Technol.*, 2018, vol. 56, pp. 313–25.
15. J.B. Kim, T.H. Lee, and I. Sohn: *Metall. Mater. Trans. A*, 2018, vol. 49A, pp. 2705–20.
16. H.L. Fan, Y.Z. Zhu, Z.F. Xu, and R.X. Wang: *J. Non-cryst. Solids*, 2022, vol. 584, p. 121482.
17. J.B. Kim and I. Sohn: *J. Non-cryst. Solids*, 2013, vol. 379, pp. 235–43.
18. S. Kou: *Welding Metallurgy*, 2nd ed. Wiley, New York, 2003, pp. 199–214.
19. X.B. Yuan, Y.W. Wu, M. Zhong, S. Basu, Z.J. Wang, and C. Wang: *Sci. Technol. Weld. Join.*, 2022, vol. 27, pp. 683–89.
20. Y.Y. Zhang, J. Zhang, H.X. Liu, Z.J. Wang, and C. Wang: *Metall. Mater. Trans. B*, 2022, vol. 53B, pp. 1329–34.
21. H.K.D.H. Bhadeshia and L.E. Svensson: *Mathematical Modeling of Weld Phenomena*, Institute of Materials, London, 1993, pp. 109–82.
22. Z.Y. Zhang and R.A. Farrar: *J. Mater. Sci.*, 1995, vol. 30, pp. 5581–88.
23. B.V. Sengupta and P.F. Mendez: *Weld. J.*, 2017, vol. 96, pp. 334s–53s.
24. D.W. Cho, D.V. Kiran, and S.J. Na: *Int. J. Heat Mass Transf.*, 2017, vol. 110, pp. 104–12.
25. D.W. Cho, W.H. Song, M.H. Cho, and S.J. Na: *J. Mater. Process. Technol.*, 2013, vol. 213, pp. 2278–91.
26. G.M. Evans: *Weld. J.*, 1983, vol. 62, pp. 313s–20s.
27. G.H. Zhang, X.F. Lu, J.Q. Li, J. Chen, X. Lin, M. Wang, H. Tan, and W.D. Huang: *Addit. Manuf.*, 2022, vol. 55, p. 102865.
28. T.D. Anderson, J.N. DuPont, and T. DebRoy: *Acta Mater.*, 2010, vol. 58, pp. 1441–54.
29. L. Cheng, X.L. Wan, and K.M. Wu: *Mater. Charact.*, 2010, vol. 61, pp. 192–97.
30. P. Dominic and D. Rian: *Metall. Mater. Trans. A*, 2004, vol. 35A, pp. 3701–06.
31. D.J. Abson: *Sci. Technol. Weld. Join.*, 2018, vol. 23, pp. 635–48.
32. A. Lambert-Perlade, A.F. Gourgues, and A. Pineau: *Acta Mater.*, 2004, vol. 52, pp. 2337–48.
33. J. Pu, S.F. Yu, and Y.Y. Li: *J. Mater. Process. Technol.*, 2017, vol. 240, pp. 145–53.
34. H.J. Hu, G. Xu, M. Nabeel, N. Dogan, and H.S. Zurob: *Metall. Mater. Trans. A*, 2021, vol. 52A, pp. 817–25.
35. T. Kaneshita, G. Miyamoto, and T. Furuhara: *Acta Mater.*, 2017, vol. 127, pp. 368–78.
36. X.L. Wan, H.H. Wang, L. Cheng, and K.M. Wu: *Mater. Charact.*, 2012, vol. 67, pp. 41–51.
37. H.K.D.H. Bhadeshia, L.E. Svensson, and B. Gretoft: *J. Mater. Sci.*, 1986, vol. 21, pp. 3947–51.
38. X.B. Yuan, M. Zhong, Y.W. Wu, and C. Wang: *Metall. Mater. Trans. B*, 2022, vol. 53B, pp. 656–61.
39. Y. Kang, J.H. Jang, J.H. Park, and C.H. Lee: *Met. Mater. Int.*, 2014, vol. 20, pp. 119–27.
40. S.S. Babu, S.A. David, J.M. Vitek, K. Mundra, and T. DebRoy: *Mater. Sci. Technol.*, 1995, vol. 11, pp. 186–99.
41. D. Zhang, H. Terasaki, and Y. Komizo: *Acta Mater.*, 2010, vol. 58, pp. 1369–78.